

FEDSM-ICNMM2010-30661

A Numerical Investigation for Nano-Particles Deposition in Realistic Geometry of Deviant Human Nasal Airways

Hajar Moghadas

School of Mechanical Engineering
Shiraz University, Shiraz, Iran

Omid Abouali

School of Mechanical Engineering
Shiraz University, Shiraz, Iran
abouali@shirazu.ac.ir

Abolhasan Faramarzi

Ear, Throat and Nose
Department, Shiraz University of
Medical Science, Shiraz, Iran

Behdash Tavakoli

Mechanical and Aeronautical
Engineering Department,
Clarkson University, Potsdam,
NY, USA

Goodarz Ahmadi

Mechanical and Aeronautical
Engineering Department,
Clarkson University, Potsdam,
NY, USA

ABSTRACT

3-D models of both sides of human nasal passages were developed to investigate the effect of septal deviation on the flow patterns and nano particles deposition in the realistic human nasal airways. 3-D computational domain was constructed by a series of coronal CT scan image before and after septoplasty from a live 25-year old nonsmoking male with septal deviation in his right side nasal passage. For several breathing rates corresponding to low or moderate activities, the steady state flow in the nasal passages was simulated numerically. Eulerian approach was employed to find the nano particles concentrations in the nasal channels. The flow field and particles depositions depend on the passage geometry. The abnormal passage has more particles deposition comparing with the normal side and post-operative passages for nano particles because of rapid change in geometry. However, regional depositions have the same behavior for the nano particles in the three different studied passages. Despite the anatomical differences of the human subjects used in the experiments and computer model, the simulation results are in qualitative agreement with the experimental data.

NOMENCLATURE

C	nano particle concentration
C_{in}	nano particle concentration in the inlet
D	nano particle diffusivity
DE	Deposition efficiency
Q_{in}	Inlet volume flow rate
d_p	particle diameter
K_B	Boltzmann constant
T	absolute temperature
u_i	Particle velocity
λ	air mean free path
μ	fluid viscosity

INTRODUCTION

The human nasal airways play an important role in the respiratory system. This part filters, tempers and humidifies the inspired air and protects lung from toxic particles by capturing them. The deviation in the nasal airways is a common disease which makes septoplasty one of the most often performed operations. It is desired to predict the flow patterns inside the nasal airways and its relation to geometric variation because of deviation. A detailed investigation of the flow field for the extremely complex human nasal airway can be very helpful for successful surgery in the cases of impaired respiration due to injuries or from an abnormal shape nasal airways. Even a

normal airways have a highly complex system both geometrically and functionally and as the Fig 1 shows this complexity gets more for abnormal airways. It can be referred to Croce et al (2006) who explained the nasal cavity anatomy in detailed.

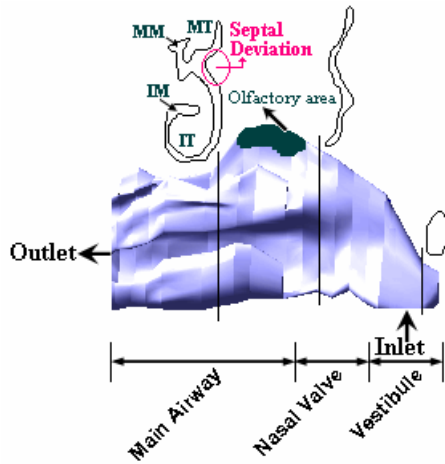


FIG. 1: Schematic of the lateral view for the right nasal cavity of a volunteer. IT and MT refer to inferior and middle turbinates. IM and MM refer to inferior and middle meatuses. It must be mentioned that the darkened grey sections represent the airways, not the cavity tissue.

Several researchers have studied flow transports through human nasal passages experimentally. Schreck et al. (1993) used a hot wire device on 3-times magnified plastic model of a nose based on MRI images. They reported that the main part of the breathing air passes through the central part of the nasal passage while only a small fraction passes through the meatuses and the olfactory region. Hahn et al. (1993) created a 20 times magnified model and used a hot film anemometer to measure the flow velocity at several points in the five coronal planes throughout the model. Their experimental study indicated that the flow was laminar up to a breathing rate of 24 L/min. Kelly et al. (2000) fabricated a model from CT scans images and used Particle Image Velocimetry (PIV) for velocity measurement. They reported that the flow was laminar for a breathing rate of 15 L/min and a significant part of the flow passes through inferior airway while a small portion of the flow passes through olfactory slit and meatuses. It was also found from their experiments that the inspired air reaches the highest velocity in the nasal valve and the inferior turbinate regions. Kim and Chang (2003) discussed the effect of geometry variation on the flow field. They studied three geometric variations of the middle turbinate experimentally and showed that the flow field was depending strongly on the geometry variation.

Some numerical studies of the flow field inside the human nasal passages have been reported in the literature by Keyhani et al. (1995), Subramaniam et al. (1998), Zhao et al. (2004), Weinhold and Mlynski (2004), Shi et al. (2006) and Wen et al. (2008).

Several researchers have studied nano particle transportation through human nasal passages experimentally and numerically. Strong and Swift (1987), Cheng et al. (1988) and Swift et al.

(1992) measured the capture of ultrafine particles in human nasal passage for different flow rates. Cheng et al. (1993) recommended an empirical relation for deposition efficiency of the human nasal passage based on particle molecular diffusivity and breathing rate for particle sizes of 1 to 200 nm. Swift and Cheng et al. (1996) carry out in vivo measurements of the ultrafine particles deposition in the human nasal passages. In their work, they also developed a modified empirical equation for the nasal deposition efficiency in terms of Reynolds number (Re), Schmidt number (Sc), and the ratio of average cross sectional area to the surface area of the nasal passage. Martonen et al. (2003) suggested a two-term formula for nasal deposition due to laminar, turbulent or transition regimes in different parts of the nasal passage. Kelly et al. (2004) measured the deposition of nano particles in nasal airway replicas created by stereo-lithography with different surface quality, SLA nasal replica model with greater surface roughness than Viper nasal replica model with smooth surface. They reported that the surface quality does not significantly affect the nasal deposition efficiency of nano particles. Scherer et al. (1994) used Eulerian-Eulerian approach to simulate uptake patterns of inhaled pollutants into the nasal passage in a laminar regime. They focused on the effect of solubility on the nasal deposition efficiency. The effects of solubility and diffusivity on the mass transfer for the wall of the passages that are covered by the mucus layer, through a first order chemical reaction model considered before. Yu et al. (1998) used an Eulerian approach to simulate the ultrafine particles deposition at a laminar constant flow rate of 15 L/min. Shi (2006) studied the transport and deposition of nano particles at transient laminar airflow. Zamankhan et al. (2006) constructed a 3-D computational model from a series of MRI images of coronal sections of a live human nose to study the flow and the transport and deposition of nano size particles in the nasal passage. They simulated the steady state flow for several breathing rates associated with low or moderate activities. Their numerical results were in qualitative agreement with the available experimental data. Liu et al. (2007), Xi and Longest (2008) and studied the total deposition of submicron aerosols with different size at several constant flow rates. The deposition efficiency increased with decreasing particle size and flow rate, indicating that diffusion was the dominant mechanism. Inthavong et al. (2009) investigated the deposition of submicron particles, particularly the nano particles and micron particles (1-10 μ m) under different steady laminar flow rates by using the Lagrangian approach. They discussed the significance and influence of different factors that are applicable to micro and nano particles and the detailed local deposition patterns.

The effect of pathologic conditions such as the presence of polyps, swelling, atrophy or resection of turbinates and for enlarged adenoids in the nasal airflow were studied with cadaver models by Tonndrof (1939), Proetz (1951), Swift and Proctor (1977). Grutzenmacher et al. (2006) study the presence of compensatory hypertrophy of turbinates. Their reports show that these conditions changed the flow patterns in the nasal cavities with different order. In addition, the detail of the investigation for the effect of the septal deviation on the flowfield inside the nasal passage in present study was brought in Moghaddas et al. (2009).

Xiong et al. (2008) simulated the nasal cavity airflow pre and post virtual functional endoscopic surgery (FESS). They selected a healthy individual, and applied CFD techniques to construct a three-dimensional nasal model based on nasal CT scans. A virtual FESS intervention was performed numerically on the normal nasal model using Fluent software. Airflow, velocity and pressure distribution calculated and compared in both pre and post FESS models. Their results showed that in the post-FESS model, there was an increase in airflow distribution in the maxillary, ethmoid and sphenoid sinuses, and a 13% increase through the area connecting the middle meatus and the surgically opened ethmoid. There was a gradual decrease in nasal resistance in the posterior ethmoid sinus region following FESS.

Chung and Kim (2008) used PDIV procedure to study nasal airflow and its change after modification of the nasal turbinates. They also investigated the flow patterns in both nasal cavities of one patient with asymptomatic deviated nasal septum. Their experimental results show that generally the flow patterns and major pathways in the middle airway were similar in both concave and convex cavities with that of airflow in the normal nasal passage. There are no published reports on the symptomatic deviated nasal septum. While the normal nasal septum would be a straight midline structure between right and left nasal passages, most of people have some degree of twist or irregularity of the nasal septum. The deviated septum is presenting generally congenital, but may also be consequence accident. However, the number of symptomatic persons with deviated nasal septum is lower than that of asymptomatic patients.

In present study, several computer models of the nasal airway are developed from a human with nasal septal deviation who referred to an otolaryngologist with chief complaint of right side nasal obstruction. The flow field in the nasal passages is investigated pre and post-operatively. The nasal septum deviation causes nasal obstruction, desiccation and epistaxis. Quality of Patient life was mostly affected when the curvature of the septum makes nasal obstruction. Deviation and obstruction can occur at any point of the bony or cartilaginous septum. Nasal septum deviation becomes clinically important when it effect in functional or aesthetic morbidity. Small changes at the septum can significantly narrow the internal nasal valve, which can further result in dynamic collapse of the upper lateral cartilages.

MODEL DESCRIPTION

1. Computational model of the nasal airway

The creation of an accurate 3-D model of the airway with complex geometry is the first step for simulation of flow field in the nasal airway. Here the coronal cross sections of the nasal cavities obtained by CT scan of an adult man human subject were used to construct a smooth airway passage for the pre and post-operative cases for both sides, as shown in Fig. 2. CT scans were taken three months after the septoplasty. Details explain of the nasal passage and septal deviation of this patient was presented by Moghadas et al. (2009).

The major deviation is located in the main airway region. Septal deviation started from a section with 30mm distance from the nose tip by decreasing the area of the airway.

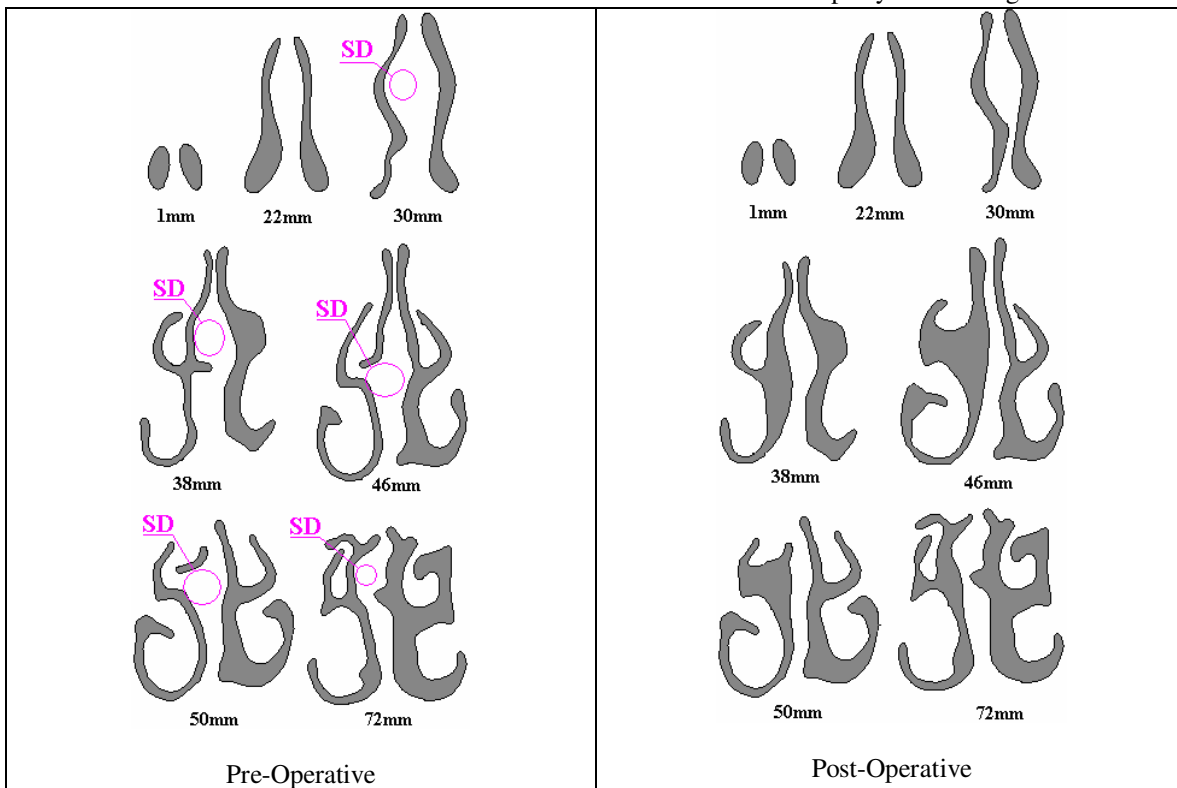


FIG. 2: Left and right 2-D coronal cross sections for a nasal passage of an adult human at various distances from the nose tip. The patient had a septal deviation in the right side pre-operatively. SD refers to the septal deviation. The patient had a septal deviation in the right side pre-operatively. It must be mentioned that the darkened grey sections represent the airways, not the cavity tissue.

Pink circles reveal the deviation position in the right side of septum, a bone-tissue that separated left and right nasal cavity. It's worth mentioning that the darkened grey sections represent the airways, not the cavity tissue and the white-free space is septum. In the nasal valve region, asymmetry between the left and right cavity is clear which is because of deviation. In the beginning of the main airway region at 46mm distance from the nose tip, deviation has divided the right airway to two separated parts. This continued to the section with 50mm distance from the nose tip. Deviation decreased the cross sections area and the total volume of the passage. This in turn has caused some breathing problem for the patient. Two separated parts reunite again in the section with 72mm distance from the nose tip but in a different manner compared with the left side cavity. The deviation ended in the beginning of nasopharynx. In fact, the coronal cross sections distanced 2 mm apart were used to produce a 3-D model. Fig. 2 shows only some selected sections. As it can be seen, two separated parts of the airway in the right side were changed in the septoplasty to integrated airway. The right side cavity looks like somewhat a normal passage post-operatively. The left side volume was approximately 36.7 percent greater than the right side volume pre-operatively while this difference decreases to 15 percent after surgery. Therefore, 16 percent of the obstruction has been removed after septoplasty.

For generation of accurate 3-D model from 2-D coronal cross sections, it is necessary to be well-informed of real geometry of nasal airway. Since the coronal sections in the main airway have complex geometries especially for the abnormal nasal airways, creation of the 3-D passage from the coronal sections was both difficult and time consuming. The complexity of the reconstruction process has been also reported before by Kimbell (2001) and Zamankhan et al. (2006) who used different methods and also studied normal nose.

The 3-D geometry of human nasal airways was reconstructed in four steps. At first step, CT-Scan images with proper resolutions from a male volunteer with septal deviation in the right cavity pre-operatively were taken. In the second step using MATLAB software, CT-Scan images with DICOM format were processed and the boundary coordinates of the walls of the nasal cavities were identified. Then in the third step, the outcome of the image processing was imported into CATIA software and the nasal airway volume was created. Final 3D volume from CATIA was exported to mesh generation software GAMBIT to produce a 3D computational domain. The generated unstructured computational grid includes approximately 800,000 tetrahedral elements. Several finer computational grid sizes were also used for investigating the effects of grid refinements on the computational results by checking the velocity in 5 various optional points. It was validated that the numerical results are independent from the grid size for a computational grid with 600,000 cells or more. The initial generated grids generally had high skewness because of the complexity of the nasal passages. A high amount of task was done to decrease this skewness and this resulted in a better convergence in numerical solutions and decreases the error residuals of the computations. The

FLUENT^(6.3.12) software was used in order to simulate the airflow and particle transport and deposition.

2. Governing Equations and Boundary conditions

As noted before, the experimental studies of Swift and Proctor (1977), Hahn et al. (1993) and Kelly et al. (2000) have revealed that the flow in the nasal cavity is laminar for low to moderate activities corresponding to a breathing rate of 15 L/min or less. In present study, the airflow in the nasal cavity for low to moderate activities was of interest. Therefore, a laminar flow regime was assumed. While particle concentration was low and the airflow transports the particles, but the effect of particle's activities on the flow was neglected, a so-called one-way coupling was used. In this approach, the airflow field was first simulated, and then the trajectories of individual particles were calculated. As it was explained before the detail of the governing equations and flow field were reported by Moghaddas et al. (2009).

The nano particle transport and deposition calculation were performed by an Eulerian approach:

$$\frac{\partial}{\partial x_j}(u_j C) = \frac{\partial}{\partial x_j} \left[D \frac{\partial C}{\partial x_j} \right] \quad (1)$$

In Equation (1), u_j is the particle velocity, C is nano particle concentration, D ($D = \frac{k_B T C_{slip}}{3\pi\mu d_p}$) is nano particle diffusivity,

k_B is Boltzmann constant, T is the absolute temperature of air.

$$C_{slip} \left(C_{slip} = 1 + \frac{2\lambda}{d_p} \left[1.257 + 0.4 \exp\left(-1.1 \frac{d_p}{2\lambda}\right) \right] \right) \quad \text{is the}$$

Cunningham slip correction factor, λ is the air mean free path, d_p is the particle diameter, μ is the fluid viscosity.

Nano particle deposition efficiency is obtained by below equation:

$$DE = \sum_{i=1}^{n_w} \left[-A_i D \frac{\partial C}{\partial n} \Big|_i \right] / (Q_{in} C_{in}) \quad (2)$$

In Equation (2), DE refers to Deposition efficiency, A_i is the sell area on the nasal passages wall where the nano particle deposit. n is the normal direction to the wall. Q_{in} is the inlet volume flow rate and C_{in} is nano particle concentration in inlet.

For the passage wall, a no slip flow boundary condition was used and the concentration of nano particle at the wall set as zero. At the nostril and at the outlet (the beginning of nasopharynx) pressure boundary conditions were set. A zero gage pressure was set at the nostril and various negative gage pressures were set at the outlet.

RESULT AND DISCUSSION

1. Flow field simulation

The Reynolds numbers in three passages based on the average velocity and hydraulic diameter of the nostril is in the range of 100-450 for all studied cases. As mentioned in the previous studies the flow regime is laminar for these ranges of Reynolds number that is correspond to the rest inspiration in a normal nasal cavity. The flow could not be turbulent in the abnormal shape cavity in this condition because as it will be illustrated later, the velocity magnitude of the abnormal shape cavity is less than that of a normal cavity in the same pressure difference. Fig. 3 shows the stream lines of airflow inside the cavities pre and post-operatively.

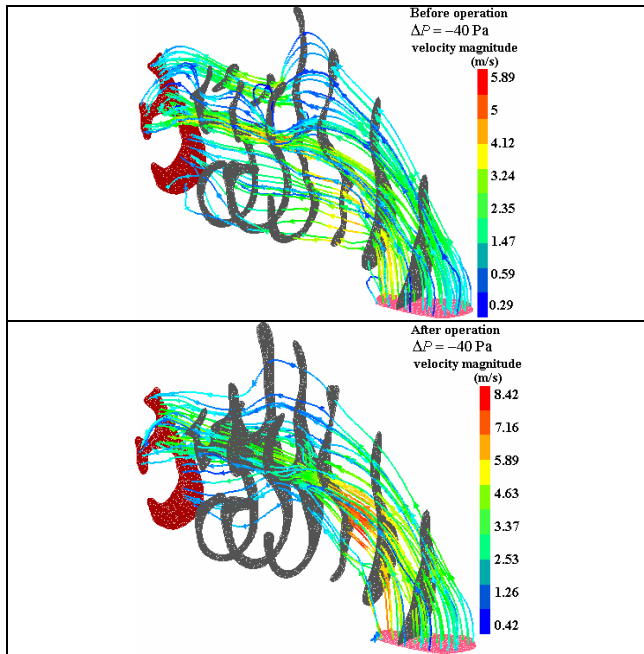


Fig. 3: The stream lines of the airflow inside the cavities pre and post-operatively for 40 Pa pressure difference.

Air flow enters from the nostril to the vestibule region and turns 90 degree to the nasal valve region then reaches to the main airway region. The stream lines expanded through the passages before operation while they contracted after operation and most of the flow passes through the middle of passage. Also after septoplasty the mass flow rates have increased which results in a higher velocity too.

The mass flow rates for various pressure differences, in the right cavity pre and post-operatively and the left cavity are compared in Fig. 4. As the results show for the same pressure difference, the amount of the flow passing through the right cavity before septoplasty is much smaller than that of the right cavity after septoplasty. However, the right post-operatively passage has approximately a breathing rate as equal as that for the normal left cavity. For this patient, at given pressure differences, the nasal airflow distinction of the abnormal right cavity before septoplasty and the left normal cavity were approximately 40 to 50 percent. Nevertheless, after septoplasty the distinction reaches to 5.6 percent and less for these cavities.

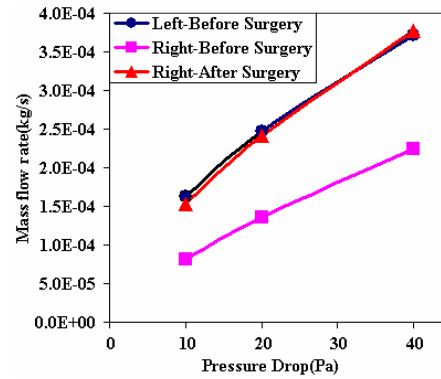


Fig. 4: The air mass flow rates in the right cavity before and after the septoplasty and the left cavity, for various pressure drops in the nasal passages.

2. Particles deposition

2.1 Total Nano particles deposition:

Distribution and deposition of nano particles were investigated by an Eulerian approach. The deposition efficiency of nano particles is compared with experimental data of Kelly et al (2004) in the Fig.5. In this study the submicron particles deposition efficiency is close to Kelly et al. (2004) data. As the results reveal, as the sizes of nano particles increase, deposition efficiency decreases because of the random motion weakens for larger particles. This behavior is observed in all three different passages with completely different geometries. Difference of the deposition efficiency in various geometries also decreases as the size of nano particle increases.

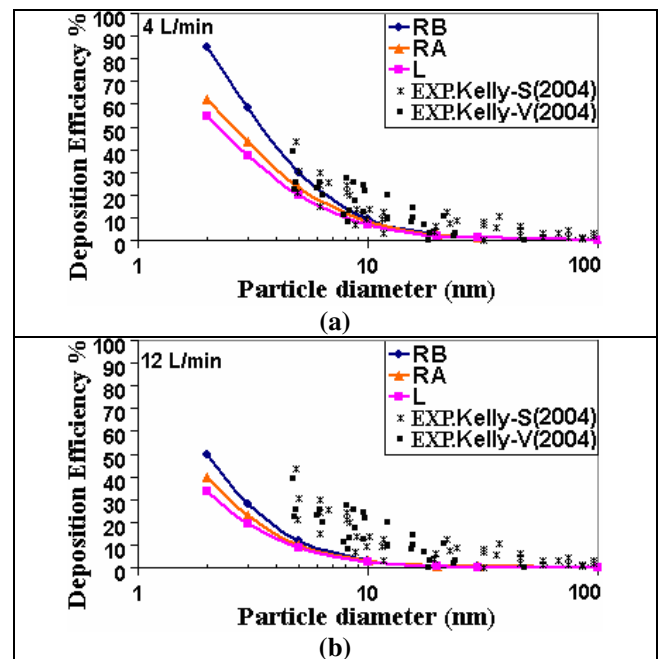


Fig.5: The deposition efficiency versus diameter of nano particles compared with the experimental data of Kelly et al (2004), the letters S and V refer to the SLA and Viper nasal replica models. RB, RA and L refer to the right cavity before operation, the right cavity after operation and the left cavity that has no change during operation.

Fig. 6 shows the deposition flux of nano particles in three passages for 2, 5 and 10 nm particles and 4 L/min flow rate. The figures have been colored by deposition flux of particles per unit area. The results show that deposition efficiency is more in the right pre-operative cavity. However, nano particle patterns are the same in there different passages. For a given

passage and constant flow rate nano particle deposition increases as the particle size decreases and for a given particle size, particle deposition decreases as the flow rate increases. Brownian motion is significant mechanism for submicron particles deposition.

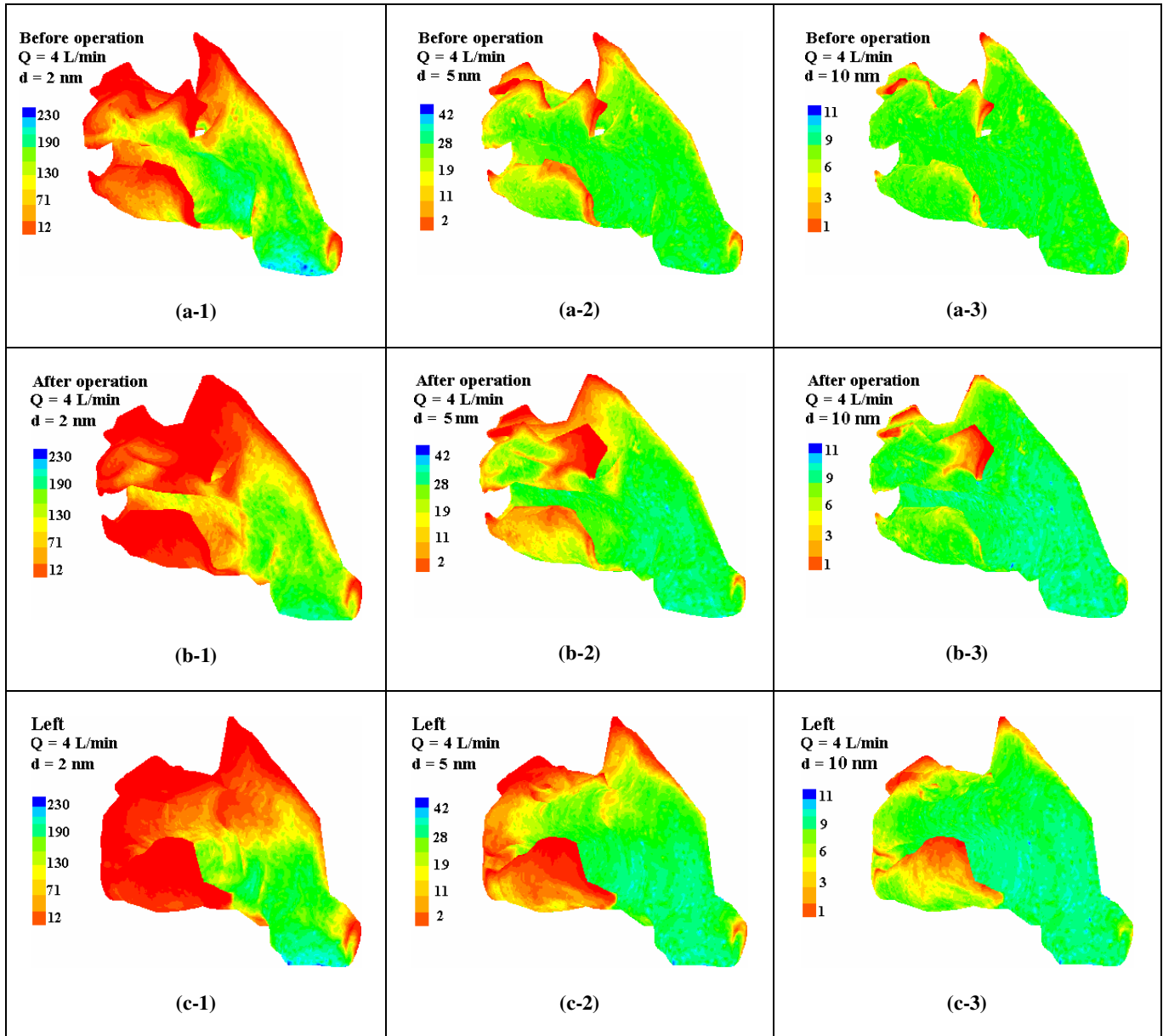


Fig.6: The deposition flux in different passages for 4 L/min and particles sizes of 2, 5 and 10 nm. First row illustrates the right pre- operation, second row corresponds to the right cavity post-operation and third row depicts the left passage that has no change during operation.

Besides, Fig.7 shows that as the flow rate increases, the difference of deposition in various passages decreases. Furthermore in a given passage decrease of the flow rate and increase of the particle size will decline deposition in the nasal passage and so more penetration to the oral airway and lung will happen. This is not desirable since the penetrated particles may deposit there and cause some diseases for respiratory system.

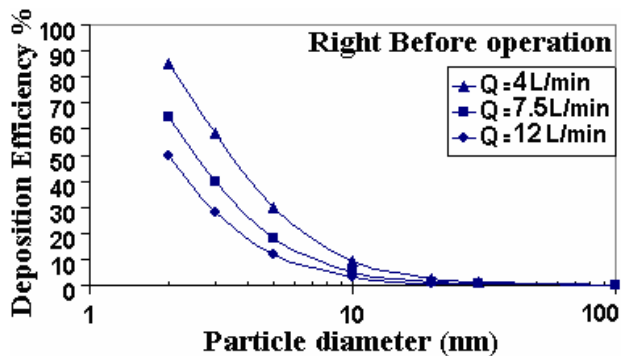


Fig.7: The deposition efficiency versus diameter of nano particles for various volume flow rate in a given passage. (Here right pre-operatively cavity).

Comparisons with the other numerical results are shown in the Fig.7. There are some scatters in the experimental data of Kelly et al. (2004) for both the SLA and the Viper models. Zamankhan et al. (2006) presented a good result for particles smaller than 20 nm but for particles larger than 20 nm, the deposition efficiency was higher than the average of the experimental data. They justified this discrepancy with the numerical errors and the anatomical differences in the nasal passages used in different works. Xi and Logest (2008) constructed their numerical model using the the same set of nasal images of Kelly et al. (2004). They showed that a drift flux particle transport model with near-wall velocity corrections could provide an effective approach in simulating the transport and deposition of nano particles in human nasal airways.

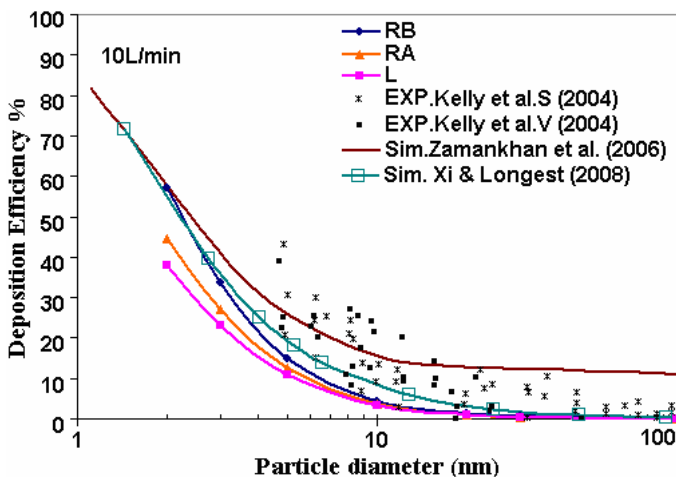


Fig.7: Comparisons of deposition efficiency of nano particles with the earlier numerical results and experimental data, the letters S and V refer to the SLA and Viper nasal replica models.

The result of present study is similar to the Xi and Logest's (2008) work and is in good agreement with experimental data of Kelly et al. (2004) especially for the particles greater than 20 nm where deposition efficiency approximates zero. The biggest distinction between the right pre and post-operatively with Kelly et al. (2004) data's is less than 10% and 20% respectively. The anatomical differences in the nasal passages used in different works might be the biggest source of dissimilarity. In spite of some differences, there are the analogous pattern for the results of this study and the experimental data.

2.2 Local deposition of nano particle:

Local deposition of 2, 5 and 10 nm particles at 4 and 12 L/min flow rate are compared in the Fig.8. As it's seen in the figure, for the right pre-operative cavity the highest deposition occurs in the main airway region because of its larger area compared to the other regions and its deviation. For nano particles, the nasal valve region has more particle deposition compared to the vestibule region. Also as the nano particles size or flow rate increase, the deposition efficiency decreases. Care should be taken for these specific sizes of nano particles because toxic particles can pass through the nasal system filtration and reach to the upper airway and lung. This can be dangerous for the inspiration system. Fig.8 depicts that the local nano particles deposition is nearly similar before and after septoplasty. However, the amount of particle deposition decreases after septoplasty. As Fig.8(c-1, c-2) shows the nano particles deposition in the left cavity is also similar to two other passages. Therefore, the results show that nano particles deposition is less affected by the geometry. In fact, Brownian motion of nano particle is less affected by complexity of geometry.

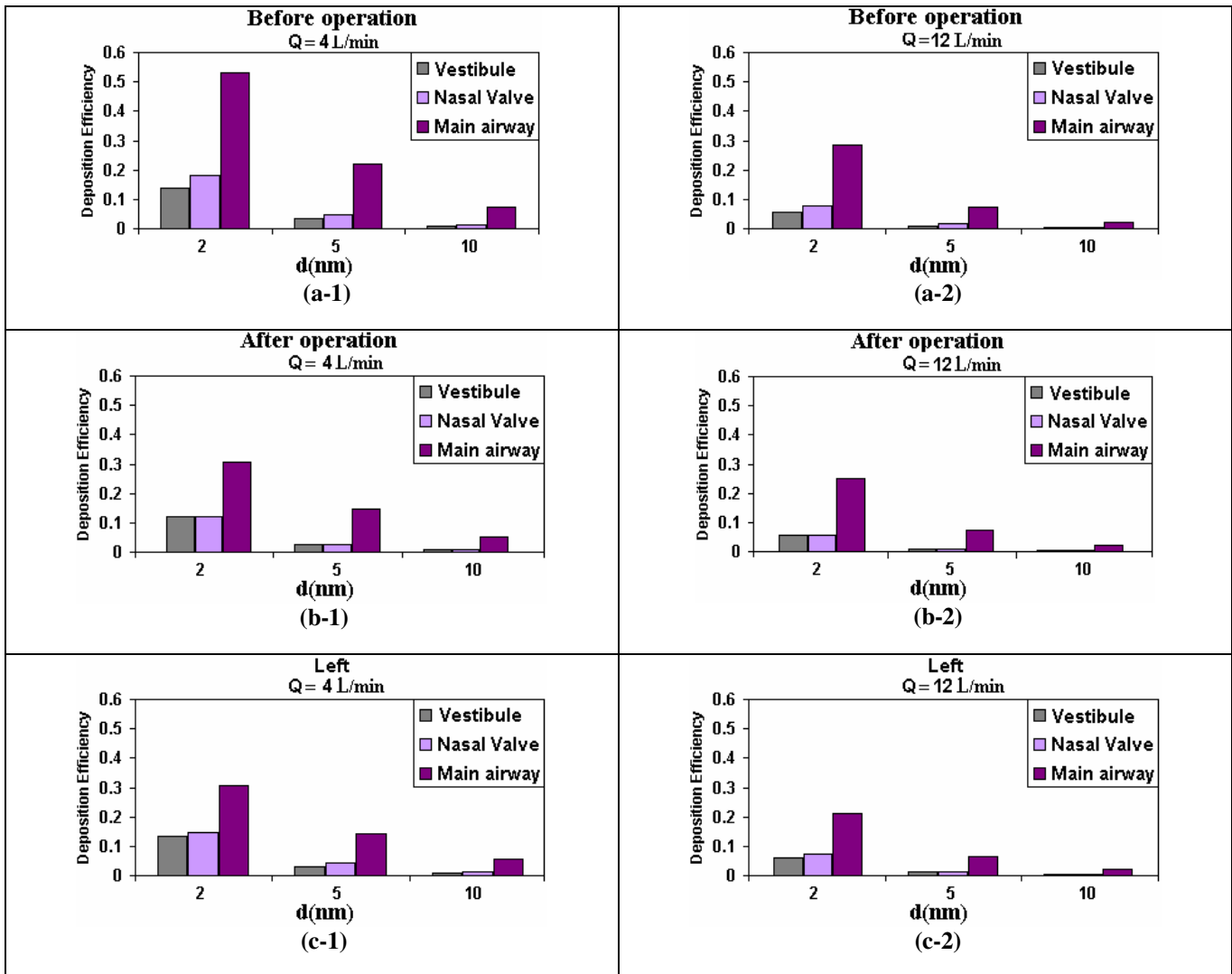


Fig.8: The local deposition efficiency of 2, 5 and 10 nm particles at 4 and 12 L/min flow rate.

CONCLUSIONS

The following conclusions can be cited from the present computer simulation.

1. The amount of the breathing rate in the studied abnormal human nasal cavity is approximately 40-50 percent less than that of a normal human nasal cavity.
2. After an appropriate septoplasty for an abnormal shape cavity, the nasal airway can have the breathing rates as equal as the normal nasal cavity.
3. The abnormal shape passage has more particles deposition compared with the normal passages because of rapid change in geometry.
4. As it was expected deposition efficiency of nano-particles decreases as their size increase and flow rate. Because the Brownian motion is the dominant force for this range of particle sizes.
5. Maximum deposition decreases 20% for 2 nm particles after septoplasty for a typical volume air flow rate.
6. The nano particles regional depositions have a similar trend in different passages.

In the current study laminar flow regime for septal deviated nose and nano particles deposition were simulated. Heavier activities and exercise induce higher breathing rates, which may persuade the turbulent flow in the nasal passage. In this situation, the influence of turbulence perturbation on particle distribution needs to be mixed up in the analysis. Also the abnormality may happen in somewhere else, like turbinate. Above all the local particle release is very prominent in drug delivery. This extra assay is left for a future study.

REFERENCES

- [1] Tonndorf, J. Der weg der atemluft in der menschlichen nase. Arch. Ohren. Nasen Kehlkopfheilkd 146, 41–63. 1939.
- [2] Proetz, A.W., Air currents in the upper respiratory tract and their clinical importance. Ann. Otol. Rhinol. Laryngol. 60, 439–467. 1951.
- [3] Swift, D.L., Proctor, D.F. Access of air to the respiratory tract. In: Brain, J.D., Proctor, D.F., Reid, L.M. (Eds.),

Respiratory Defence Mechanisms. Part 1. Marcel Dekker, New York, NY, pp. 63–93. 1977.

[4] Cheng, Y.S., Yamada, Y., Yeh, H.C., and Swift, D.L. Diffusional Deposition of Ultrafine Aerosols in a Human Nasal Cast. *J. Aerosol Sci.* 19(6), pp. 741–751. 1988.

[5] Swift, D.L., Montassier, N., Hopke, P.H., Karpen-Hayes, K., Cheng, Y.S., Su, Y.F., Yeh, H.C. and Strong, J.C. Inspiratory deposition of ultrafine particles in human nasal replicate cast. *J. Aerosol Sci.* 23(1),65-72. 1992.

[6] Cheng, Y.S., Su, Y.F., Yeh, H.C. and Swift, D.L. Deposition of Thoron Progeny in Human Head Airways. *Aerosol Science and Technology*. Vol. 18, pp. 359–375. 1993.

[7] Hahn, I., Scherer, P.W. and Mozell, M.M. Velocity profiles measured for airflow through a large-scale model of the human nasal cavity. *J. Appl. Physiol.* Vol. 75, pp. 2273–2287. 1993.

[8] Schreck,S., Sullivan, K.J., Ho, C.M. and Chang, H.K. Correlations between Flow Resistance and Geometry in a Model of the Human Nose. *J. Appl. Physiol.* 75:1767–1775. 1993.

[9] Scherer, P.W., Keyhani, K., and Mozell, M.M. Nasal Dosimetry Modeling for Humans. *Inhaled Toxicol.* Vol. 6, pp. 85–97. 1994.

[10] Keyhani, K., Scherer, P.W. and Mozell, M.M. Numerical simulation of airflow in the human nasal cavity. *J. Biomech. Eng.* Vol. 117, pp. 429–441. 1995.

[11] Swift, D.L. and Strong, J.C. Nasal deposition of ultrafine 218 Po Aerosols in human subjects. *J. Aerosol Sci.* 27(7),1125-1132. 1996.

[12] Cheng, Y.S., Yeh, H.C., Guilmette, R.A., Simpson, S.Q., Cheng, K.H., and Swift, D.L. Nasal Deposition of Ultrafine Particles in Human Volunteers and Its Relationship to Airway Geometry. *Aerosol Sci. Technol.* 25:274–291. 1996.

[13] Subramaniam, R.P., Richardson, R.B., Morgan, K.T., Kimbell, J.S., and Guilmette, R.A.. Computational Fluid Dynamics Simulations of Inspiratory Air flow in the Human Nose and Nasopharynx. *Inhal. Toxicol.* 10, 91–120. 1998.

[14] Yu, G., Zhang, Z., and Lessmann, R. Fluid Flow and Particle Diffusion in the Human Upper Respiratory System. *Aerosol Science and Technology*. Vol. 28, pp. 146–158. 1998.

[15] Kelly, J.T., Prasad, A.K. and Wexler, A.S. Detailed flow patterns in the nasal cavity. *J. Appl. Physiol.* Vol. 89, pp. 323–337. 2000.

[16] Kimbell, J.S. Computational Fluid Dynamics of the Extrathoracic Airways. *Medical Applications of Computer Modelling: The Respirator System*, MarTonen, T. B. (ed). WIT Press, Southampton, UK. 2001.

[17] Kim, S.K. and Chung, S.K. An investigation on airflow in disordered nasal cavity and its corrected models by tomographic PIV, *Meas. Sci. Technol.* Vol. 15, pp. 1090–1096. 2003.

[18] Martonen, T.B., Zhang, Z., Yue, G., and Musante, C.J. Fine Particle Deposition Within Human Nasal Airways. *Inhaled Toxicol.* Vol. 15, pp. 283–303. 2003.

[19] Kelly, J.T., Asgharian, B., Kimbell, J.S., and Wong, B.A. Particle Deposition in Human Nasal Airway Replicas Manufactured by Different Methods. Part II: Ultrafine

Particles, *Aerosol Science and Technology*. Vol. 38, pp. 1072–1079. 2004.

[20] Weinhold, I., and Mlynski, G. Numerical simulation of air flow in the human nose. *European Archives of Otorhinolaryngology*, 261, 452–455. 2004.

[21] Zhao, K., Scherer, P.W., Hajiloo, S.A., and Dalton, P. Effect of anatomy on human nasal air flow and odorant transport patterns implications for olfaction. *Chemical Senses*, 29(5), 365–379. 2004.

[22] Croce, C., Fodil, R., Durand, M., Sbirlea-Apiou, G., Caillibotte, G., Franc, J., Papon, O., Blondeau, J. R., Coste, A., Isabey, D., and Louls, B. In Vitro Experiments and Numerical Simulations of Airflow in Realistic Nasal Airway Geometry. *Annals of Biomedical Engineering*. Vol. 34, pp. 997–1007. 2006.

[23] Grützenmacher, S., Robinson, D.M., Grafe, K., Lang, C., Mlynski, G. First findings concerning airflow in noses with septal deviation and compensatory turbinate hypertrophy—a model study. *ORL J. Otorhinolaryngol. Relat. Spec.* 68, 199–205. 2006.

[24] Shi, H., Kleinstreuer, C., and Zhang, Z. Laminar airflow and nanoparticle or vapor deposition in a human nasal cavity model. *ASME Journal of Biomechanical Engineering*, 128, pp. 697–706. 2006.

[25] Zamankhan, P., Ahmadi, G., Wang, Z., Hopke, P.K., Cheng, Y.S., Su, W.C. and Leonard, D. Air flow and Deposition of Nano-Particles in a Human Nasal Cavity. *Aerosol Sci. Technol.* 40, 463–476. 2006.

[26] Liu, Y., Matida, E. A., Gu, J., and Johnson, M.R. Numerical simulation of aerosol deposition in a 3-D human nasal cavity using RANS, RANS/EIM, and LES. *Aerosol Science*. Vol. 38, pp. 683 – 700. 2007.

[27] Chung, S.K. and Kim, S.K. Digital Particle image velocity studies of nasal airflow. *Respiratory Physiology & Neurobiology*. Vol. 163, pp. 111–120. 2008.

[28] Wen, J., Inthavong, k., Tu, T., and Wang, S. Numerical simulations for detailed airflow dynamics in a human nasal cavity. *Respiratory Physiology & Neurobiology*, 125–135. 2008.

[29] Xi, J. and Longest, P. W. Numerical predictions of submicrometer aerosol deposition in the nasal cavity using a novel drift flux approach. *International Journal of Heat and Mass Transfer*. Vol. 51, pp. 5562–5577. 2008.

[30] Xiong,G., Zhan, J., Zuo, K., Li, J., Rong., L. and Xu., G. Numerical flow simulation in the post-endoscopic sinus surgery nasal cavity. *International Federation for Medical and Biological Engineering*. 46:1161–1167. 2008.

[31] Inthavong, K., Wang, S., Wen, J., Tu, J and Xue, C. Comparison of micron and nano particle deposition patterns in a realistic human nasal cavity. in J. Goh (ed.) 3th International Conference on Biomedical Engineering Proceedings, Singapore, 3-6 December 2008. 2009.

[32] Moghadas, H., Abouali, and O., Faramarzi, A. Numerical Simulation of Flow Field in Realistic Geometry of Human Nasal Airways with Septum Deviation. 17th International Conference on Mechanical Engineering ISME2009, Iran, Tehran, 19-21 May 2009. 2009.